2010 International Conference on Electrical Machines and Systems

October 10-13, 2010, Songdo Convensia, Incheon, Korea

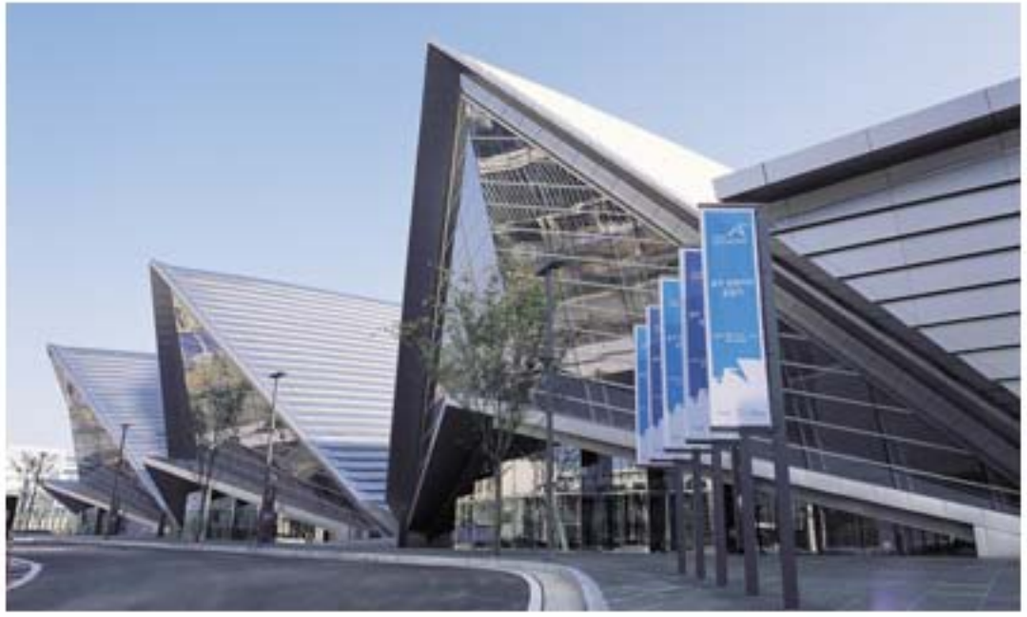

IEEE Catalog Number: CFP10801-CDR
ISBN: 978-89-86510-12-6
Vendor: Prof. Jin Hur
Tel: +82-52-259-1282 / Fax: +82-52-259-1686
E-mail: jinhur@ulsan.ac.kr

Organized by

KIEE (The Korean Institute of Electrical Engineers)

Co-organized by

CES (China Electrotechnical Society)

IEEJ (The Institute of Electrical Engineers of Japan)

Technical Co-sponsor

IEEE IEEE Industry Application Society

Jung Pyo Hong

- Influence of Materials on Design of Interior PM Synchronous Motor

Jung Pyo Hong

- Optimal Shape Design of Double-barriers in Single-layer Interior PM Synchronous Motor for Reducing Torque Pulsation

Jung Sik Choi

- Efficiency Optimization Control of SynRM Drive Using Multi-AFLC

Jung Sik Choi

- High Performance Control of Induction Motor Drive using HIPI Controller

Jung Sik Choi

- Maximum Power Point Tracking Control of Photovoltaic System Using Neural Network

Jung Sik Choi

- A Novel Tracking Method for a High Efficiency of PV Generation Considering Shaded Conditions

Jung Woo Baek

- High Performance Control of Induction Motor Drive using HIPI Controller

Influence of Materials on Design of Interior PM Synchronous Motor

Yong Ho Kim, Sun Tao, Soon O Kwon, Jung Pyo Hong
Department of Automotive Engineering, Hanyang University
E-mail: hongjp@hanyang.ac.kr

Abstract — This paper studies the influence of core material on the design of the interior PM synchronous motor (IPMSM). Two kinds of ferromagnetic steels are selected in this paper. And with these two core materials, two IPMSMs used to drive the electric scooter are designed. First, the parameters of these two motors, including the inductance, iron-loss resistance, and back electromotive force are calculated in the numerical methods. Then, using the equivalent circuit, the characteristics such as current, efficiency, copper loss and iron losses are estimated. Finally, for the same output power, the dimension, weight and cost of these two motors will be compared. The study results of this paper will provide the reference of core material selection to the various designs of motor.

I. INTRODUCTION

In the design of motor, the selection of core material is the first step and the most important step [1]. For achieving high efficiency, the low iron-loss ferromagnetic steel usually is used. In order to reduce the iron losses, the thickness of steel and area of hysteresis loop per cycle should be much reduced so that the eddy current loss and the hysteresis loss can be minimized. The special manufacture process and material however make the low iron-loss steel much more expensive. Additionally, the low iron-loss steel is not perfect. They are more easily saturated than those having higher iron losses. Therefore, the volume and weight may be larger when use these materials [2].

Based on these characteristics, there are compromises for the selection of core material as the different applications. In this paper, two kinds of silicon steels are studied. One is 35A230 model which has relatively low iron losses and low saturation flux density. The other is 50A1300 model which has the relatively high iron losses and high saturation flux density. The B-H curves and iron losses (@ 3 kHz) curves of these two silicon steel are compared in Fig. 1 (a) and (b), respectively. In order to reveal the influence of the ferromagnetic steel on the design of the motor, using these materials, two interior PM synchronous motors (IPMSM) are designed. First, the parameters of these two motors are calculated in a series of numerical methods. The influence of material on the inductance, iron-loss resistance and back electromotive force (Back-EMF) can be investigated. Then, using the equivalent circuit, the characteristics of these two motors can be estimated. As the same output power, the current, efficiency, power factor, copper loss, and iron losses can be compared in the result. Next, the maximum torque of these two motors will be calculated in the finite element method (FEM) considering the influence of iron-loss resistance. Based on the results, the volume, weight and cost will be approximately calculated and compared. The result of this paper will provide reference of core material selection to the various designs of motor.

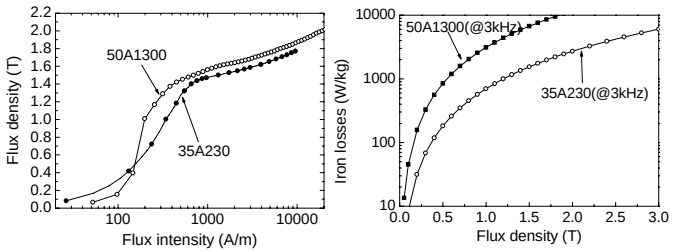

Fig. 1. Material data of 35A230 and 50A1300 silicon steel: (a) B-H curve, (b) iron losses data (@3 kHz)

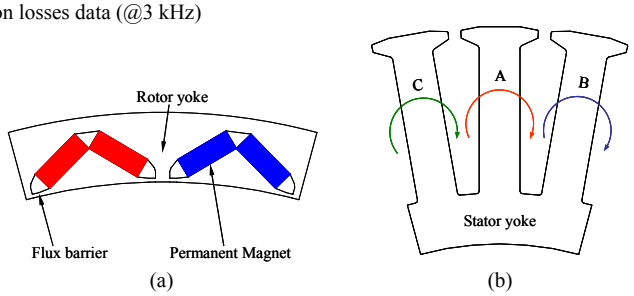

Fig. 2. Cross-section of analysis model with winding arrangement: (a) 1/12 rotor model, (b) 1/12 stator model with winding arrangement.

II. ANALYSIS MODEL

In this paper, the analyzed model is an in-wheel direct drive traction motor for the electric scooter. Due to the fine cooling condition, the current density of this motor is allowed to be 15A/mm^2, which may cause a significant saturation issue. The cross-section of this motor is shown in Fig. 2. And Fig. 3 shows the design requirement for the torque vs. speed and power vs. speed characteristics in maximum power and rated power operation, respectively. It can be seen that this motor should achieve the maximum torque of 138Nm, the maximum speed of 700rpm, the maximum power of 2.8kW and rated power of 1.5kW. In order to produce this extremely high torque in the restricted volume, the large number of pole is decided. And considering the vibration effect, the ratio of the number of pole and slot is chosen to 2/3.

III. PARAMETER CALCULATION AND COMPARISON

In order to accurately estimate the influence of material on the parameters of motor, the numeric methods are used. The dominate parameters includes back-EMF, iron-loss resistance, and inductances will be calculated in a series of finite element methods.

A. Magneto-static Field Analysis and Back-EMF

The current vector control has been used in various applications, especially in the IPMSM, which is used to ach-

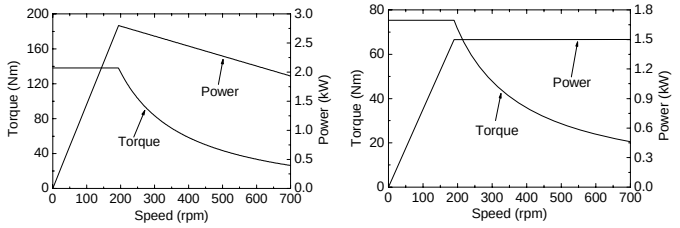

Fig. 3. Required torque and power: (a) maximum power operation, (b) rated power operation.

ieve the maximum torque per ampere control and field weakening control [3]. Therefore, it is convenient to use the magneto-static field analysis method to calculate the parameters. The governing equation of magneto-static field for the IPMSM, i.e. the nonlinear Possion equation, can be described as

$$\nabla \times \upsilon\left(\nabla \times \boldsymbol{A}\right) = \boldsymbol{J} + \nabla \times \left(\upsilon \mu_0 \boldsymbol{M}\right) \tag{1}$$

where $\boldsymbol{A}$ is the magnetic potential vector, $\boldsymbol{J}$ is the current density vector, $\boldsymbol{M}$ is the magnetization vector, and $\boldsymbol{\upsilon}$ is the reluctivity of permanent magnet. The flux density then can be directly calculated by the obtained $\boldsymbol{A}$. Fig. 4 shows the calculated Back-EMF waveforms in 1000rpm of the analysis model using the 50A1300 and 35A230 materials, respectively.

B. Iron losses Calculation and Iron-loss Resistance

In this paper, a method which was proposed and verified in [3] is used to calculate the iron losses. First, using the magneto-static field analysis, the flux density of each element can be calculated. Then, the frequency and amplitude of these flux densities are analyzed in the Discrete Fourier Transform (DFT) as described in (2).

$$B_{pk}(k) = \sum_{n=0}^{N-1} B_p(n) e^{j(2\pi nk)/N} \tag{2}$$

where k is harmonic order, N is the number of the discrete data, $B_{pk}(k)$ is the amplitude of magnetic flux density of the k^{th} harmonic, and $B_p(n)$ is magnitude of the point n (n=0, 1, …,N-1). When the frequencies and amplitudes of magnetic flux density at each element are obtained, depending on them, the iron losses at each element are calculated from an iron loss data sheet that is tested by the Epstein test apparatus. Then, sum the results of all harmonics and all elements, the total iron loss can be obtained.

At the end, the equivalent iron-loss resistance is calculated by (3)

$$R_c = \frac{v_0^2}{P_c} \tag{3}$$

where v_0 is the back-EMF calculated at each speed, Pc is the corresponding iron losses. In this method, the iron-loss resistance with different materials are calculated and compared in Fig. 5.

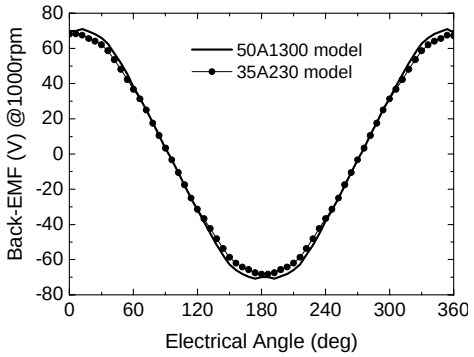

Fig. 4. Comparison of Back-EMF waveforms for different materials.

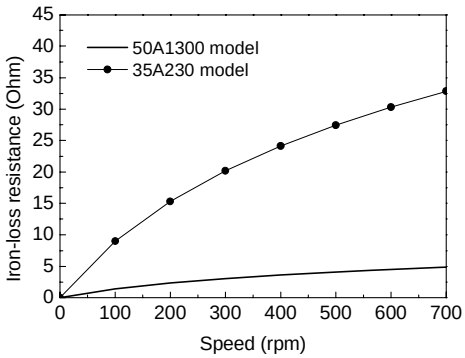

Fig. 5. Comparison of iron-loss resistances for different materials.

C. d- and q-axis Inductances Calculation

The inductance calculation method used in this paper is described in [4]. A phasor diagram of the IPMSM is shown in Fig. 6. In the solid-line part, it can be seen that there are the relationships (4)

$$L_d = \frac{\psi_0 \cos\alpha - \psi_a}{i_d}$$
$$L_q = \frac{\psi_0 \sin\alpha}{i_q} \tag{4}$$

where ψ_a is the flux linkage generated by the permanent magnet, ψ_0 is the combined flux linkage produced by the permanent magnet and excited armature current, and the α is the phase shift between these two flux linkages. The calculated inductances with different current magnitude and vector angle are shown in Fig. 7.

As shown in Fig. 1 (a), the material 35A230 has lower flux density for the same magnetomotive force (MMF). Therefore, the motor using this material has lower Back-EMF as shown in Fig. 4. In Fig. 1 (b), it can be seen that the material 50A1300 has much higher iron losses for the same flux density and frequency. Because of the similar magnitude of Back-EMF, the higher iron losses lead to the lower iron-loss resistance, which is coincident with Fig. 5. In Fig. 7, the d- and q-axis inductances of 50A1300 model are slightly smaller than those of 35A230 model. This seems to be contrary to the characteristic of B-H curves. In fact, in the 35A230 model, due to the serious saturation on the rotor, the flux produced by the armature winding passes through the slot rather than

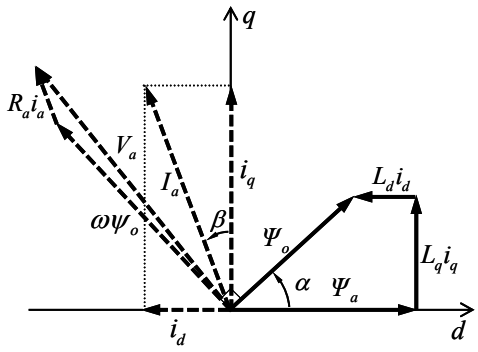

Fig. 6 Phasor diagram of IPMSM

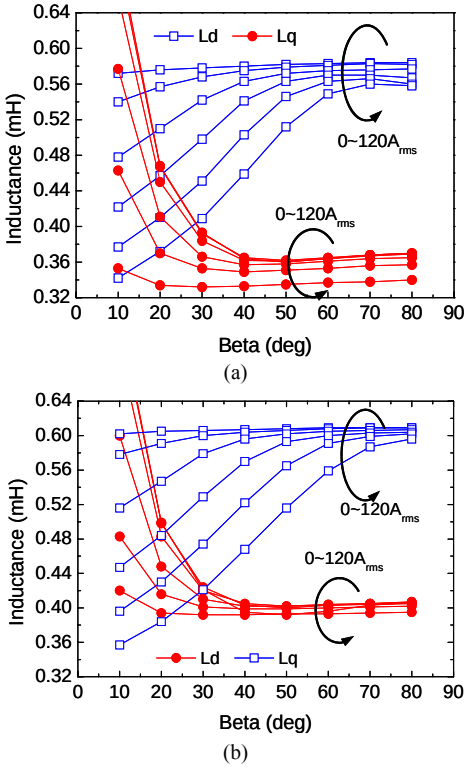

Fig. 7 d- and q-axis inductances: (a) inductances of 50A1300 model; (b) inductances of 35A230 model.

passes through the rotor, i.e. the large leakage flux is produced. Because the reluctance between the teeth is smaller than that of PM, the higher inductances are produced in the 35A230 model.

IV. Characteristic Analysis and Comparison

A. d- and q-axis Equivalent Circuit

According to the Park transformation, the IPMSM can be described in the equivalent circuits as shown in Fig. 8 [3]. The corresponding voltage equations of these two circuits can be expressed in

$$\begin{bmatrix} v_d \\ v_q \end{bmatrix} = R_a \begin{bmatrix} i_{od} \\ i_{oq} \end{bmatrix} + \left(1+\frac{R_a}{R_c}\right)\begin{bmatrix} v_{od} \\ v_{oq} \end{bmatrix} + p\begin{bmatrix} L_d & 0 \\ 0 & L_q \end{bmatrix}\begin{bmatrix} i_{od} \\ i_{oq} \end{bmatrix} \quad (5)$$

and $$\begin{bmatrix} v_{od} \\ v_{oq} \end{bmatrix} = \begin{bmatrix} 0 & -\omega L_q \\ \omega L_d & 0 \end{bmatrix}\begin{bmatrix} i_{od} \\ i_{oq} \end{bmatrix} + \begin{bmatrix} 0 \\ \omega\psi_a \end{bmatrix}$$

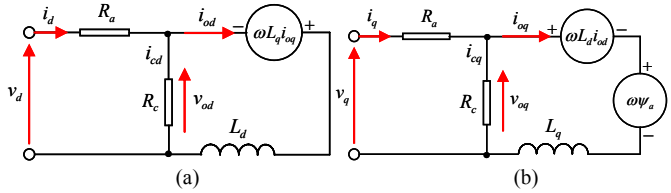

Fig.8. Equivalent circuit of IPMSM: (a) d-axis circuit, (b) q-axis circuit

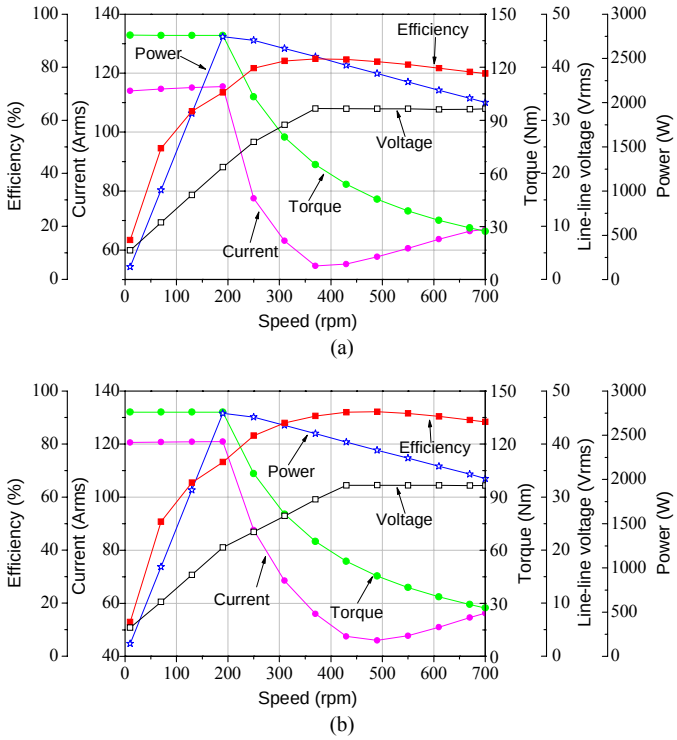

Fig.9. Characteristics: (a) 50A1300 model, (b) 35A230 model.

And the torque, losses and efficiency can be calculated in

$$T = P\left[\psi_a i_{od} + \left(L_d - L_q\right) i_{od} i_{oq}\right] \quad (6)$$

$$P_c = R_a I_a^{\,2} = R_a (i_d^{\,2} + i_q^{\,2}) \quad (7)$$

$$P_i = \frac{V_o^{\,2}}{R_c} = \frac{\omega^2\left[(L_d i_{od} + \psi_a)^2 + (L_q i_{oq})^2\right]}{R_c} \quad (8)$$

$$P_m = P_w + P_f = 2D^2 L\omega^3 + K_f M\omega^3 \quad (9)$$

$$\eta = \frac{T\cdot\omega}{T\cdot\omega + P_c + P_i + P_m} \quad (10)$$

where R_a is the phase winding resistance, R_c is the iron-loss resistance, P is the number of pole pair, ω is the electrical angular velocity, i_{od} and i_{oq} are the d- and q-axis load currents, P_c, P_i, P_m are the copper loss, iron losses and mechanical losses, respectively, D is the outer radii of rotor, L is the stack length of motor, K_f is the friction factor, and M is the mass of rotor.

The major parameters, such as the inductances, iron-loss resistance, and flux linkage can be obtained in the previous introduced methods. Depending on this equivalent circuit, the characteristics of these two models are estimated and

compared in Fig. 9. It can be observed that the current of the 35A230 model is larger than that of the 50A1300 model before the base speed, while it is smaller than that of the 50A1300 model after the base speed. This is because the number of turns in series connection of the 35A230 model is reduced in order to decrease both Back-EMF and inductances to achieve the optimized efficiency for fare comparison. The detail comparisons at the typical operation points are shown in Table I.

TABLE I
COMPARISON OF CHARACTERISTICS (@190 RPM AND 138NM)

	Current (A_{rms})	Efficiency (%)	Copper Loss (W)	Iron Losses (W)
50A1300 model	103	73	894	138
35A230 model	121	73	977	26

COMPARISON OF CHARACTERISTICS (@700 RPM AND 27NM)

	Current (A_{rms})	Efficiency (%)	Copper Loss (W)	Iron Losses (W)
50A1300 model	67	78	384	181
35A230 model	57	88	215	41

COMPARISON OF CHARACTERISTICS (@420 RPM AND 34NM)

	Current (A_{rms})	Efficiency (%)	Copper Loss (W)	Iron Losses (W)
50A1300 model	39	80	126	253
35A230 model	31	93	63	51

*190rpm is base speed; 420rpm is rated operation speed.

According to this analysis results, the maximum torque of these two models are calculated in FEM. The results are compared in Fig. 10. The mean value of the maximum torque of the 35A230 model is 131Nm that is smaller than that of the 50PN1300 model although they have the same maximum torque value in the results of the equivalent circuit analysis. This is mainly because the 35A230 material is easier to be saturated. In order to get higher torque, the stack length of the 35A230 model has to be increased. Finally, the specifications of these two models are determined and listed in Table II. And the maximum torque of the improved 35A230 model is shown in Fig, 10.

TABLE II
SPECIFICATION OF ANALYSIS MODEL

Terms	Value		Unit
	50A1300 model	35A230 model	
Battery voltage	48		V
Maximum / Rated power	2.8 / 1.5		kW
Maximum current	105	125	A_{rms}
Outer diameter of rotor	234		mm
Inner diameter of stator	205		mm
Air gap / stack length	0.7 / 64	0.7 / 69	mm
Volume of PM	5632	6072	mm^3
No. of turns in series connection	64	50	
No. of parallel circuit	6		
Phase resistance	33.7	22.7	mΩ

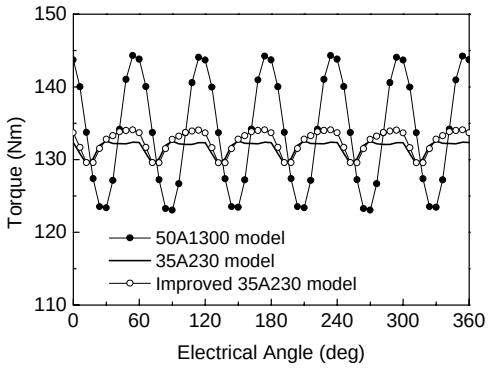

Fig.10. Comparison of the maximum torques calculated in FEM.

In Table I, it can be seen that in the MTPA operation region, the efficiency of both models are same. As speed increases, the 35A230 model behaviors higher efficiency characteristics. At the rated power operation, the efficiency of 35A230 model is higher than that of 50A1300 model by 13%. The major loss of the 50PN1300 model is the iron losses which is 4 times of that of the 35A230 model and 2 times of own copper losses. The shortage of the high iron losses material is obvious at this point.

On the other hand, the maximum current of 50A1300 model is lower than that of 35A230 model by 15%. In fact, as shown in Table II, it can be seen that the maximum current of 35A230 model is increased from $121A_{rms}$ to $125A_{rms}$ in order to overcome the saturation effect on the maximum torque generation. Although the higher current does not increase the copper loss because of the lower phase resistance, the total system efficiency will be influenced. As known, the capacity of battery is described in A·H. It implies that the higher current will shorten the battery discharging time and hence shorten the distance of electric scooter. Also, the higher discharge current will much increase the copper loss of battery. In addition, the modern AC motor drive uses the switching device for the DC-DC converter and inverter. The losses of these switching devices are proportional to the switching frequency as well as the conducting current. These issues will be evaluated in the further study.

Finally, according to the dimensions of these two models, the weight and cost are calculated and compared in Table III. The cost of 35A230 material is regarded as 1 US dollar per kilogram in Asian, and it is about 1.5 times of that of 50A1300. The rare earth permanent magnet is used in this paper. Until 2007 its price is about 15 US dollar per kilogram. Certainly, due to the recent national policy, the price of rare earth permanent magnet has been much increased. The winding usually is copper made. Its price is regarded as 5 US dollar per kilogram. It can be seen that the 50A1300 model is about lighter than 35A230 model by 1 kg. Although it is only about 5% of the total weight, it cause the almost 10 US dollar difference on the price that means the price is reduced by about 20%.

V. CONCLUSION

This paper studies an in-wheel direct drive traction motor using in electric scooter considering two different ferromagnetic core materials. The parameters with different

materials are calculated in numerical methods. Using these parameters, the characteristics are analyzed and compared. According to the results, the 50A1300 model, i.e. a high saturation flux density material, requires lower current compared with that using the 35A230 material. Although the 35A230 model has 13% higher efficiency at rated operation point, the total system efficiency including the battery and switching devices should be deeply discussed due to the high flowing current. Finally, the volume, weight and cost of the models using these two materials are compared. The total price of the 35A230 model is higher than that of the 50A1300 model by about 20%. The unsure total system efficiency and high cost result in a compromise on the determination of ferromagnetic core material.

TABLE III
Comparison on Volume, Weight and Cost

Terms		Value		Unit
		50A1300 model	35A230 model	
Volume	Core	0.00159	0.00171	m^3
	PM	0.000135	0.000146	m^3
Weight	Core	12.24	13.17	kg
	PM	1.03	1.11	kg
	Winding	3.94	3.82	kg
	Total	17.21	18.1	kg
Cost	Core	12	20	$
	PM	15	17	$
	Winding	20	19	$
	Total	47	56	$

REFERENCES

[1] T. A. Lipo, *Introduction to AC Machine Design,* vol. 1, WisPERC: UW-Madison, 1996, pp. 315-317.

[2] M. Nakano, K. Ishiyama, etc., "Reduction of Iron Loss in Thin Grain-Oriented Silicon Steel Sheets", *IEEE Transaction on Magnetics*, vol. 33, no. 5, Sept. 1997.

[3] Tao Sun, Jung-Pyo Hong, etc., "Determination of Parameters of Motor Simulation Module Employed in ADVISOR", *IEEE Transaction on Magnetics*, vol. 44, no. 6, Jun. 2008.

[4] Tao. Sun, Jung-Pyo Hong, etc., "Investigation and Comparison of Inductance Calculation Methods in Interior Permanent Magnet Synchronous Motors", in Proc. 2008 IEEE *Electrical Machines and Systems, Conf.*, pp. 3131-3136.